Oncogene (2010) 29, 5254–5264

www.nature.com/onc

ORIGINAL ARTICLE

An anti-Axl monoclonal antibody attenuates xenograft tumor growth and enhances the effect of multiple anticancer therapies

X Ye[1,5], Y Li[1,5], S Stawicki[2], S Couto[3], J Eastham-Anderson[3], D Kallop[4], R Weimer[4], Y Wu[2] and L Pei[1]

[1]*Department of Molecular Oncology, Genentech Inc., South San Francisco, CA, USA;* [2]*Department of Antibody Engineering, Genentech Inc., South San Francisco, CA, USA;* [3]*Department of Pathology, Genentech Inc., South San Francisco, CA, USA and* [4]*Department of Biomedical Imaging, Genentech Inc., South San Francisco, CA, USA*

Axl is expressed in various types of cancer and is involved in multiple processes of tumorigenesis, including promoting tumor cell growth, migration, invasion, metastasis as well as angiogenesis. To evaluate further the mechanisms involved in the expression/activation of Axl in various aspects of tumorigenesis, especially its roles in modulating tumor stromal functions, we have developed a phage-derived mAb (YW327.6S2) that recognizes both human and murine Axl. YW327.6S2 binds to both human and murine Axl with high affinity. It blocks the ligand Gas6 binding to the receptor, downregulates receptor expression, inhibits receptor activation and downstream signaling. In A549 non-small-cell lung cancer (NSCLC) and MDA-MB-231 breast cancer models, YW327.6S2 attenuates xenograft tumor growth and potentiates the effect of anti-VEGF treatment. In NSCLC models, YW327.6S2 also enhances the effect of erlotinib and chemotherapy in reducing tumor growth. Furthermore, YW327.6S2 reduces the metastasis of MDA-MB-231 breast cancer cells to distant organs. YW327.6S2 induces tumor cell apoptosis in NSCLC, reduces tumor-associated vascular density and inhibits the secretion of inflammatory cytokines and chemokines from tumor-associated macrophages in the breast cancer model. In conclusion, anti-Axl mAb can enhance the therapeutic efficacy of anti-VEGF, EGFR small-molecule inhibitors as well as chemotherapy. Axl mAb affects not only tumor cells but also tumor stroma through its modulation of tumor-associated vasculature and immune cell functions.
Oncogene (2010) **29,** 5254–5264; doi:10.1038/onc.2010.268; published online 5 July 2010

Keywords: monoclonal antibody; tumor stroma; combination therapies

Introduction

Axl belongs to a family of receptor tyrosine kinases that also includes Tyro3 and Mer (O'Bryan *et al*., 1991; Lai and Lemke, 1991). It was originally identified as a transforming gene in hematological malignancies (O'Bryan *et al*., 1991; Janssen *et al*., 1991). Dysregulation of Axl or its ligand Gas6 is implicated in the pathogenesis of a variety of human cancers. Overexpression of Axl has been reported in a wide array of human cancers (Craven *et al*., 1995; Ito *et al*., 1999; Berclaz *et al*., 2001; Sun *et al*., 2004; Shieh *et al*., 2005) and is associated with invasiveness and metastasis in lung (Shieh *et al*., 2005), prostate (Sainaghi *et al*., 2005), breast (Meric *et al*., 2002; Zhang *et al*., 2008), gastric (Wu *et al*., 2002) and pancreatic (Koorstra *et al*., 2009) cancers, renal cell carcinoma (Chung *et al*., 2003) as well as glioblastoma (Hutterer *et al*., 2008). Recently, by profiling of phosphotyrosine signaling, activated Axl protein was detected in about 5% primary tumors of non-small-cell lung cancer (NSCLC) (Rikova *et al*., 2007). Expression of Axl is induced by targeted and chemotherapy drugs and drug-induced Axl expression confers resistance to chemotherapy in acute myeloid leukemia (Hong *et al*., 2008) as well as resistance to imatinib and lapatinib/herceptin in gastrointestinal stromal tumors (Mahadevan *et al*., 2007) and breast cancer (Liu *et al*., 2009), respectively.

In a previous study, we have used RNA interference (RNAi) and human Axl-specific monoclonal antibodies (mAbs) to assess the oncogenic potential of Axl (Li *et al*., 2009). We showed that downregulation of Axl by RNAi or anti-human Axl mAbs reduces NSCLC xenograft tumor growth. Inhibition of Axl expression in MDA-MB-231 breast cancer cells attenuates their migration and inhibits their metastasis to the lung in an orthotopic model. Axl knockdown in endothelial cells impaired tube formation and this effect is additive with anti-VEGF. Further, we obtained evidence that Axl regulates endothelial cell functions by modulation of signaling through angiopoietin/Tie-2 and Dickkopf-3 (DKK3) pathways. These results showed that Axl has multiple roles in tumorigenesis, affecting tumor growth, migration, metastasis as well as angiogenesis.

Although knockdown of Axl by RNAi approach and hybridoma antibodies that recognize only human Axl (Li *et al*., 2009) provided insight into the role of Axl in tumor cells, these tools can not be used to assess the potential roles of Axl in the tumor stroma. To evaluate further the mechanisms involved in the expression/activation of Axl in

Correspondence: Dr L Pei, Department of Molecular Oncology, Genentech Inc., 1 DNA Way, South San Francisco, CA 94080, USA. E-mail: lpei@gene.comor drlinpei@yahoo.com
[5]These authors contributed equally to this work.
Received 18 March 2010; revised 18 May 2010; accepted 1 June 2010; published online 5 July 2010

various aspects of tumorigenesis, especially its roles in modulating tumor stromal functions, we have developed a phage-derived mAb that recognizes both human and murine Axl. Here we describe the generation of this antibody, designated as YW327.6S2, as well as the characterization of its effects on tumor growth, metastasis, tumor-associated vasculature and immune cells.

Results

Generation of a phage derived mAb that blocks Axl's function

To identify antibodies that cross-react with murine and human Axl, we used phage-displayed antibody libraries with synthetic diversities in the selected complementary-determining regions, mimicking the natural diversity of human IgG antibodies (Lee *et al*., 2004). Phage antibodies that bound to both human and murine Axl ECD were identified by ELISA and DNA sequencing, and antibody clones were reformatted to express full-length IgGs (Liang *et al*., 2007). A panel of full-length IgGs was then screened for their ability to inhibit Gas6-dependent growth of Baf3Axl cells (Li *et al*., 2009), and one of the clones YW327.6 was affinity-matured and purified.

Affinity-matured Axl mAb YW327.6S2 binds to both human and murine Axl with high affinity, with a K_d of about 1 nM and 545 pM, respectively (Figure 1a). This antibody also binds to cynomolgus Axl, but it does not cross-react with the related receptors Tyro3 and Mer (Figure 1b). YW327.6S2 blocks the binding of ligand Gas6 to Axl as shown in both a cell-free ELISA and on cell surface by fluorescence-activated cell sorting (FACS), in a dose-dependent manner (Figure 1c).

YW327.6S2 downregulates the expression of Axl, inhibits its activation, signaling and Gas6-dependent Baf3Axl cell proliferation

To test whether YW327.6S2 affects Axl biological functions, we first evaluated its effect on the expression and signaling of Axl. Treatment of NSCLC cell line A549 with YW327.6S2 resulted in rapid down-regulation of Axl expression on the cell surface (Figure 1d, upper panel) and this downregulation is sustained for 24 h (Figure 1d, lower panel). Gas6 treatment of H1299 NSCLC cells induces Axl phosphorylation that was inhibited when cells were pre-incubated with YW327.6S2 (Figure 1e, upper panel). Consequently, pre-incubation of H1299 cells with YW327.6S2 blocks Gas6-induced phosphorylation of the downstream signaling molecule Akt (Figure 1e, lower panel). Downregulation of Axl expression and inactivation of its signaling by YW327.6S2 potently inhibited Gas6-dependent growth of Baf3Axl cells, with an IC_{50} of 340 ng/ml (Figure 1f).

YW327.6S2 reduces A549 xenograft growth and enhances the effect of anti-VEGF

In a previous study, we showed that inhibition of Axl by either RNAi or treatment with anti-human Axl hybridoma mAbs significantly attenuated A549 NSCLC tumor growth (Li *et al*., 2009). We therefore first tested the effect of YW327.6S2 on tumor growth in this model. YW327.6S2 alone at 10 mg/kg, twice a week dosing regimen significantly reduced A549 tumor growth (Figure 2a), and this inhibitory effect is comparable to that of anti-human Axl hybridoma antibodies (Figure 2c).

Axl is expressed on endothelial cells and enhances vascular endothelial growth factor (VEGF)-induced endothelial tubule formation (Holland *et al*., 2005; Li *et al*., 2009); we tested whether anti-Axl mAb could enhance the antitumor growth property of anti-VEGF (Liang *et al*., 2006). Anti-VEGF antibody alone and YW327.6S2 alone had similar effects on A549 tumor growth (Figure 2a). Combination of the two antibodies together resulted in enhanced tumor growth inhibition compared with treatment with either antibody alone, with 30% inhibition by single agent versus 60% inhibition by the combination treatment (Figure 2a).

The animals in this study were dosed twice weekly for 60 days and followed to day 85 to examine the delay in tumor growth (the animals were removed from the study when tumor sizes exceeded 800 mm^3; no animals were removed as a result of toxicity). YW327.6S2 in combination with anti-VEGF significantly delayed tumor growth as compared with a single agent (Figure 2a). There was no tumor re-growth in the combination treatment group during the time elapsed from the last dose to the end of the experiment (day 85), which lead to survival of all the animals in this group at the end of the experiment as shown in the Kaplan–Meier plot (Figure 2b).

The anti-human Axl hybridoma mAb 12A11, which does not cross-react with murine Axl, significantly attenuated A549 xenograft tumor growth (Li *et al*., 2009); it also enhances the effect of anti-VEGF as shown in Figure 2c. This is expected as 12A11 directly inhibits tumor cell growth and anti-VEGF affects tumor vasculature.

YW327.6S2 downregulates receptor expression and induces the apoptosis of A549 tumor cells

To begin to understand the mechanisms that mediate the effect of YW327.6S2 on reducing tumor growth, we performed a pharmacodynamic study. A549 tumor-bearing mice were treated with YW327.6S2 and the tumors were excised at 0, 24, 72 and 168 h after dosing. Western blotting analysis of tumor lysates showed that expression of Axl was downregulated 24 h after antibody administration and sustained over 168 h (Figure 2d), suggesting that the antitumor growth effect of YW327.6S2 is mediated in part by downregulation of the expression of Axl.

To determine whether YW327.6S2 has direct effect on tumor cell proliferation and apoptosis, A549 xenograft tumors treated with control or YW327.6S2 for 2 weeks were excised and cleaved caspase-3 and Ki67 immunohistochemistry (IHC) were performed. Tumors treated with YW327.6S2 showed increased cleaved caspase-3 as

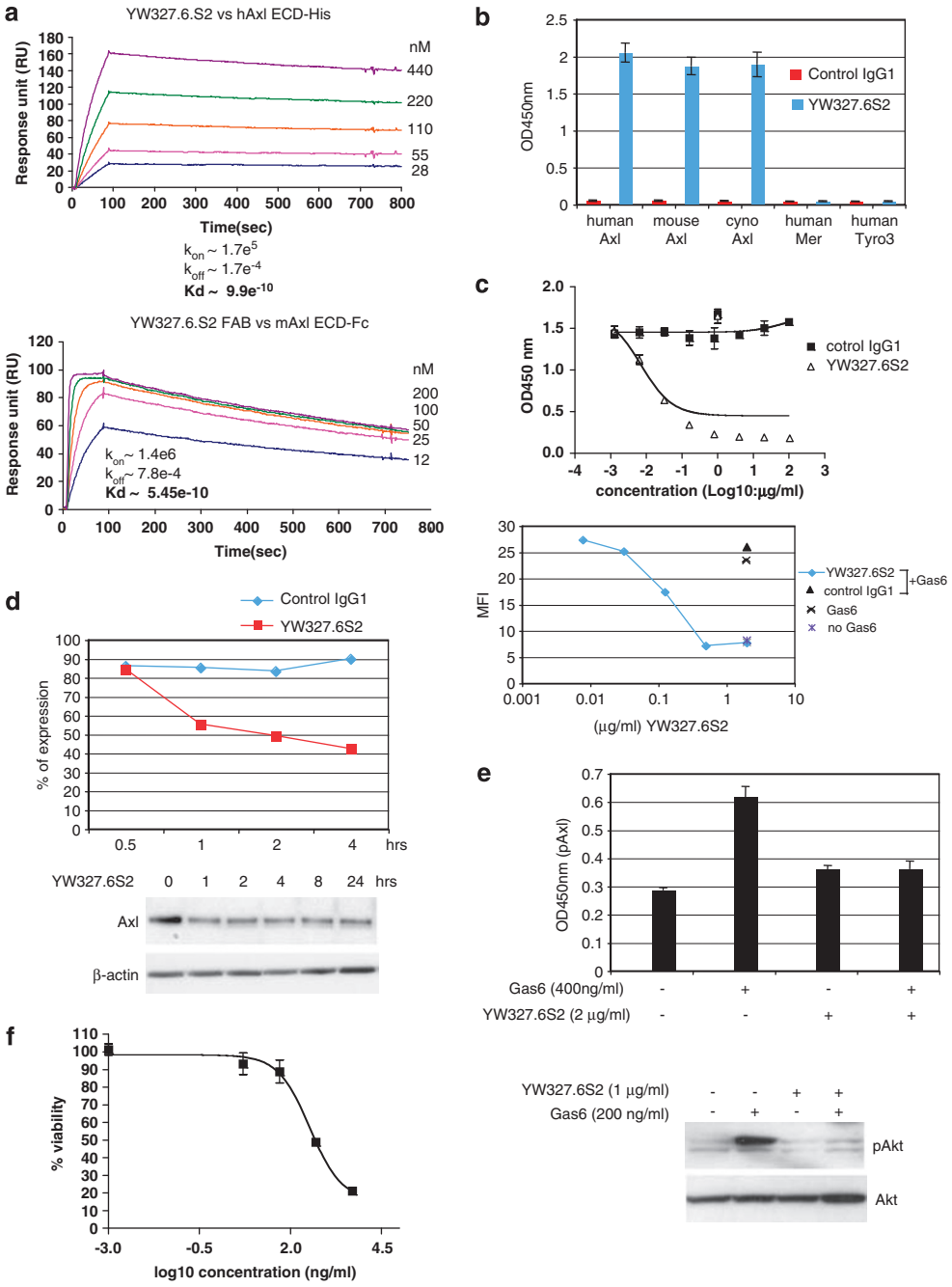

Figure 1 Characterization of Axl mAb YW327.6S2. (**a**) Affinity measurement of YW327.6S2 using BIAcore. Association rates (k_{on}) and dissociation rates (k_{off}) were calculated using the one-to-one Langmuir binding model. The equilibrium dissociation constant (K_d) was derived as the k_{on}/k_{off} ratio. (**b**) Cross-reactivity of YW327.6S2. YW327.6S2 cross-reacts with murine and cynomolgus Axl but not with Tyro3 or Mer. Plates were coated with anti-human IgG Fc and then incubated with human Axl, Mer, Tyro3 Fcs, mouse or cynomolgus Axl Fcs. After washing, an isotype control antibody or YW327.6S2 was added and followed by addition of HRP-conjugated anti-human IgG. (**c**) YW327.6S2 blocks Gas6 binding to Axl. Upper panel: ELISA. Plates were coated with anti-human IgG Fc and incubated with human Axl-Fc. After washing, Gas6 was added with or without antibodies. Binding of Gas6 was detected by biotylated anti-Gas6 antibody and streptavidin-HRP conjugate. Lower panel: FACS. HUVECs were harvested and treated with YW327.6S2 or a control antibody and then incubated with Gas6 for 30 min on ice. Binding of Gas6 to the cell surface was detected by biotinylated an anti-Gas6 antibody and streptavidin–PE conjugate. (**d**) YW327.6S2 downregulates the expression of Axl. A549 cells were incubated with 1 µg/ml YW327.6S2 for indicated time and cell-surface Axl expression was determined by FACS (upper panel), and total protein expression by western blotting analysis (lower panel). (**e**) YW327.6S2 inhibits Gas6-induced Axl phosphorylation and signaling. H1299 cells were cultured in serum free medium over night, preincubated with YW327.6S2 for 4 h and treated with Gas6 for 30 min. Phosphorylated Axl was measured by ELISA (upper panel) and phosphorylated Akt by western blotting analysis (lower panel). (**f**) YW327.6S2 inhibits the growth of Baf3Axl cells. Baf3Axl cells were grown in medium containing 200 ng/ml Gas6 and treated with YW327.6S2 at the indicated concentrations for 72 h. Cell viability was measured by CellTiter Glo assay. FACS, fluorescence-activated cell sorting; HRP, horseradish peroxidase; HUVEC, human umbilical vein endothelial cell; mAb, monoclonal antibody; PE, phycoerythrin.

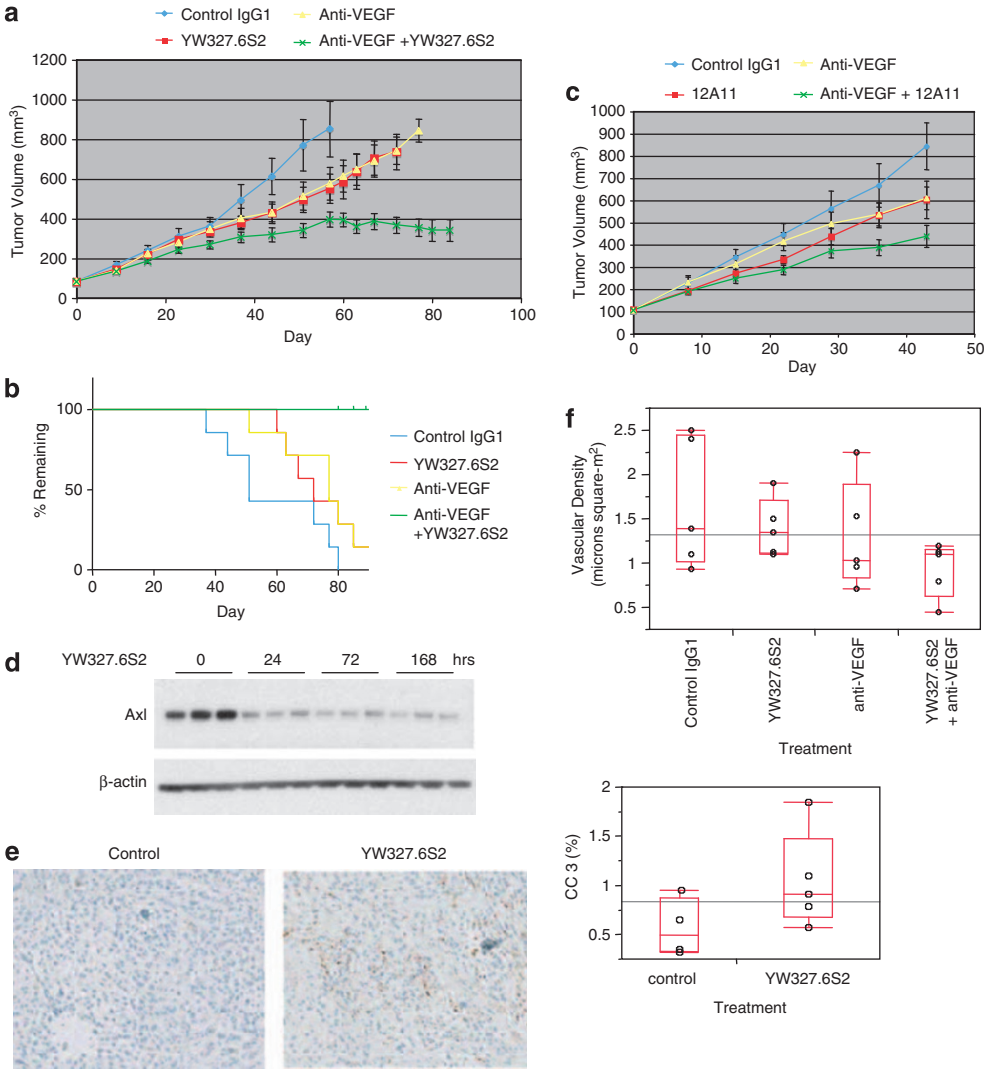

Figure 2 YW327.6S2 attenuates A549 xenograft tumor growth and enhances the effect of anti-VEGF. (**a**) Tumor growth curve. mAbs were administrated intraperitoneal injection at 10 mg/kg (YW327.6S2 and isotype control antibody) or 1 mg/kg (anti-VEGF), twice a week, starting when the mean tumor size reached 100 mm^3 (day 0). The error bars represent the standard error of the mean ($n = 10$ for each group in each experiment). $P = 0.0003$ (YW327.6S2 versus control), $P = 10^{-11}$ (YW327.6S2 versus combination). (**b**) Kaplan–Meier curve of various treatment groups. Mice were removed from the study when their tumor size reached 800 mm^3 and the animals remaining in each group (% remaining) were plotted. (**c**) 12A11 enhances the effect of anti-VEGF. 12A11 and anti-VEGF were administrated by intraperitoneal injection at 30 and 1 mg/kg, respectively, twice a week, starting when the mean tumor size reached 100 mm^3 (day 0). The error bars represent the standard error of the mean ($n = 10$ for each group in each experiment). $P = 0.006$ (12A11 versus control); $P = 0.0001$ (12A11 versus combination). (**d**) YW327.6S2 down-regulates Axl expression. Mice were treated with YW327.6S2 at 10 mg/kg and tumors excised at the indicated time points. Cell lysates from tumors were analyzed by western blot for Axl expression. (**e**) YW327.6S2 induces apoptosis. Tumors treated with control or YW327.6S2 for 2 weeks were excised and cleaved caspase-3 IHC was performed to measure apoptosis. (**f**) YW327.6S2 enhances the effect of anti-VEGF in reducing intra-tumoral vascular density. Tumors from mice treated as above in panel **d** were excised at 0 and 72 h after dosing and tumor vasculature was visualized by staining with MECA32 immunohistochemistry and quantified by image analysis (expressed as microns square). Student's *t*-test was performed for each pair ($P < 0.05$ for control versus combination). IHC, immunohistochemistry; VEGF, vascular endothelial growth factor.

compared with the control (Figure 2e), suggesting that YW327.6S2 induces apoptosis of tumor cells. There was no significant difference in Ki67-positive nuclei between control and YW327.6S2-treated tumors (data not shown), suggesting that YW327.6S2 does not directly affect tumor cell proliferation.

To investigate whether YW327.6S2 affects tumor-associated vasculature, we treated A549 tumor-bearing mice with YW327.6S2 alone or in combination with anti-VEGF. Tumors were excised and stained with MECA32, a pan endothelial marker, to examine the intratumoral vascular density. YW327.6S2 alone did not

significantly reduce vascular density as compared with the control but a combination with anti-VEGF resulted in significant decrease of the tumor-associated vascular density (Figure 2f). By contrast, 12A11 has no significant effect on intratumoral vascular density by itself or in combination with anti-VEGF (data not shown).

YW327.6S2 enhances the effect of erlotinib and chemotherapy

To test whether YW327.6S2 could enhance the therapeutic index of standard care for NSCLC, we performed combination treatment of YW327.6S2 with epidermal growth factor receptor (EGFR) small-molecule inhibitor (SMI) erlotinib and chemotherapy.

A549 contains wild-type EGFR and is only moderately sensitive to erlotinib (Yauch *et al*., 2005); we therefore investigated whether anti-Axl mAb can sensitize these cells to EGFR SMI. YW327.6S2 and erlotinib when administered as a single agent resulted in 30% reduction in tumor growth, but in combination reduced the tumor growth rate by more than 50% (Figure 3a), suggesting that anti-Axl mAb enhances the antitumor growth effect of erlotinib.

We then investigated whether anti-Axl mAb was able to enhance the therapeutic index of standard chemotherapy for NSCLC. Mice bearing A549 xenografts were treated with one cycle of chemotherapy consisting of paclitaxel (6.25 mg/kg/day, 5 days) and carboplatin (100 mg/kg, one dose) administered at the beginning of treatment (day 0; Figure 3b). Chemotherapy alone has similar effect on tumor growth as YW327.6S2 administered alone, and a combination of the two, resulted in enhanced inhibition of tumor growth (Figure 3b).

YW327.6S2 reduces vascular density and inhibits inflammatory cytokine secretion from tumor-associated macrophages in MDA-MB-231 breast cancer xenograft model

As knockdown of Axl by short-hairpin RNA has only moderate effect on MDA-MB-231 xenograft tumor growth (Li *et al*., 2009), we asked whether YW327.6S2 is efficacious in this model. YW327.6S2 alone was able to reduce tumor growth (25%), and had similar effect to anti-VEGF used as a single agent in this model (Figure 4a). The combination therapy leads to a 50% reduction in tumor growth, suggesting that YW327.6S2 potentiates the effect of anti-VEGF (Figure 4a). In contrast, the anti-Axl hybridoma antibody 12A11 (Li *et al*., 2009) which does not cross-react with murine Axl, has no significant effect on tumor growth as a single agent in this model, nor does affects anti-VEGF (Figure 4b). Western blot analysis showed that both

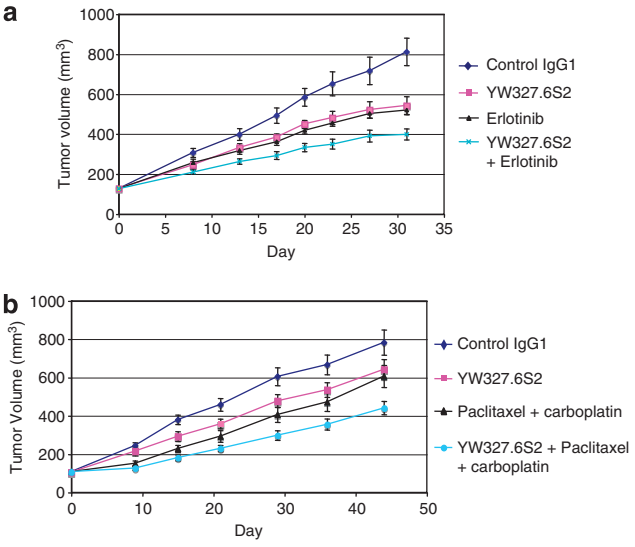

Figure 3 YW327.6S2 enhances the antitumor effect of erlotinib and chemotherapy in an A549 xenograft model. (**a**) YW327.6S2 enhances the effect of erlotinib. Antibody administration was the same as in Figure 2. Erlotinib was administered by oral gavage at 100 mg/kg/day ($n = 10$ for each group). $P = 1.7 \times 10^{-9}$ (YW327.6S2 versus control); $P = 2.3 \times 10^{-10}$ (YW327.6S2 versus combination). (**b**) YW327.6S2 enhances chemotherapy. Antibody administration was the same as in Figure 2. Paclitaxel and carboplatin were administrated subcutaneously at 6.25 mg/kg/day for 5 days, and 100 mg/kg for a single dose at the beginning of the treatment (day 0), respectively ($n = 10$ for each group). $P = 3 \times 10^{-5}$ (YW327.6S2 versus control); $P = 10^{-9}$ (chemotherapy versus control); $P = 10^{-5}$ (combination versus chemotherapy alone).

Figure 4 YW327.6S2 attenuates MDA-MB-231 xenograft tumor growth by modulating tumor stromal functions. (**a**, **b**) YW327.6S2 but not 12A11 reduces MDA-MB-231 tumor growth and enhances the effect of anti-VEGF. mAbs were administrated intraperitoneal injection at 20 mg/kg (YW327.6S2 and isotype control antibody), 30 mg/kg (12A11) and 2 mg/kg (anti-VEGF), twice a week, starting when the mean tumor size reached 100 mm^3 (day 0). Error bars represent standard error of the mean ($n = 10$ for each group in each experiment). $P = 8.5 \times 10^{-6}$ (YW327.6S2 versus control); $P = 2.8 \times 10^{-8}$ (YW327.6S2 versus combination); $P = 0.05$ (12A11 versus control); $P = 0.145$ (anti-VEGF versus combination). (**c**, **d**) YW327.6S2 downregulates expression of Axl. Mice bearing MDA-MB231 xenograft tumors (average size 500 mm^3) were treated with mAbs at 20 mg/kg and tumors excised at the indicated time points. Cell lysates from tumors were used in western blot analysis for expression of Axl. (**e**) YW327.6S2 reduces the density of tumor-associated vasculature. Tumors from mice treated as above in panel **c** were excised at 0 h and 1 week after dosing and tumor vasculature was visualized by staining with MECA32 immunohistochemistry and quantified by image analysis (expressed as microns square). Student's *t*-test was performed for each pair ($P < 0.05$ for YW327.6S2 versus control; anti-VEGF versus control and anti-VEGF versus combination). (**f**) Axl is highly expressed in infiltrating macrophages of primary human breast cancer. IHC was used to examine 79 primary tumors; 21% of these tumors express high levels of Axl in the infiltrating macrophages. Macrophages were identified by staining with anti-CD68 and expression of Axl on macrophages was determined by anti-Axl/CD68 dual IHC. Serial sections were used. (**g**) YW327.6S2 inhibits inflammatory cytokine/chemokine secretion from tumor-associated macrophages. Mice bearing MDA-MB231 xenograft tumors (average size 500 mm^3) were treated with control antibody, YW327.6S2 or 12A11 at 20 mg/kg and tumors excised after 1 week of treatment. TAMs were isolated by sorting for F4/80-positive cells and cultured overnight. Cytokines and chemokines secreted into the medium were measured using a Bio-Plex mouse cytokine assay kit. IHC, immunohistochemistry; mAb, monoclonal antibody; TAMs, Tumor associated macrophages; VEGF, vascular endothelial growth factor.

YW327.6S2 and 12A11 down-regulate Axl expression in tumors (Figures 4c and d). These results suggest that the anti-tumor growth effect of YW327.6S2 might be mediated by modulation of tumor stromal functions.

To investigate further how YW327.6S2 might modulate tumor stromal functions, we treated MDA-MB-231 tumor bearing mice with YW327.6S2 alone or in combination with anti-VEGF. At various time points after administration of the antibodies, tumors were excised and stained with MECA32 to examine the intratumoral vascular density. Both YW327.6S2 and anti-VEGF significantly reduced vascular density compared with control (Figure 4e). And combination of the two antibodies resulted in further reduction of the tumor associated vascular density. These results suggest that YW327.6S2 reduces MDA-MB-231 tumor growth in part by altering vascular functions.

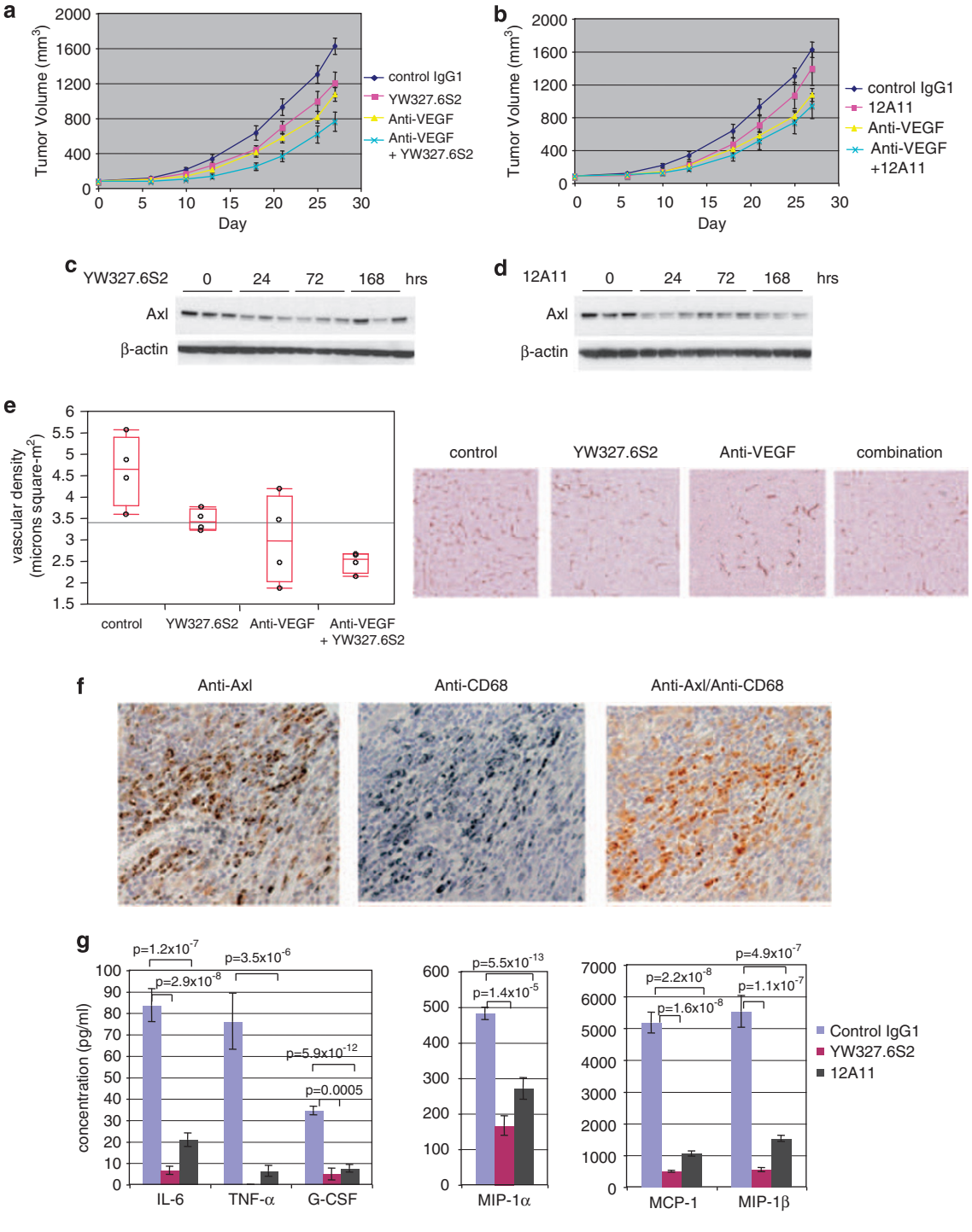

In primary human breast cancer specimens, we found that Axl protein is strongly expressed in infiltrating macrophages (Figure 4f) and therefore asked whether Axl mAb YW327.6S2 might affect tumor-associated macrophages (TAMs) functions. MDA-MB-231 xenograft tumors were treated for 1 week with YW327.6S2, 12A11 or a control antibody, and TAMs were isolated by sorting for F4/80-positive cells. Cells were cultured in serum-free media overnight and the supernatant was collected and assayed for the presence of various cytokines and chemokines. TAMs from tumors treated with YW327.6S2 and 12A11 produced much lower levels of inflammatory cytokines and chemokines as compared with TAMs treated with a control antibody (Figure 4g). Treatment with either Axl mAb does not affect the Axl expression levels on the TAMs (data not shown) in contrast to downregulation of the expression of Axl on tumor cells by theses antibodies (Figure 4c and d). These results suggest that Axl mAbs most likely modulate inflammatory cytokine/chemokine secretion from TAMs in an indirect manner, perhaps by blocking the crosstalk between tumor and stromal cells.

YW327.6S2 reduces the metastasis of MDA-MB-231 breast cancer cells to the bone

In a previous study we showed that knockdown of Axl by short-hairpin RNA inhibits the metastasis of MDA-MB-231 breast cancer cells to the lung in an orthotopic model (Li *et al*., 2009), we therefore tested whether YW327.6S2 affects the metastasis of these cells. MDA-MB-231 cells stably expressing the luciferase reporter gene (20) were injected through the tail vein into severe combined immunodeficient (SCID) mice. Four weeks after injection, strong luminescent signals were detected at the craniofacial region, the tibia and the femur of all five animals in the control antibody-treated group. The sites detected by bioluminescence in the control groups were 5, 5, 4, 3 and 1 in each animal, making a total of 18 (Figure 5a). In mice treated with YW327.6S2, the sites detected by bioluminescence were significantly reduced, with 0, 1, 2, 3 and 1 sites in each animal and a total of seven for the entire group (Figure 5a). The presence of metastatic foci in bone was verified by histological analysis (Figure 5b). These results suggest that YW327.6S2 is able to reduce the metastasis of MDA-MB-231 breast cancer cells to distant organs.

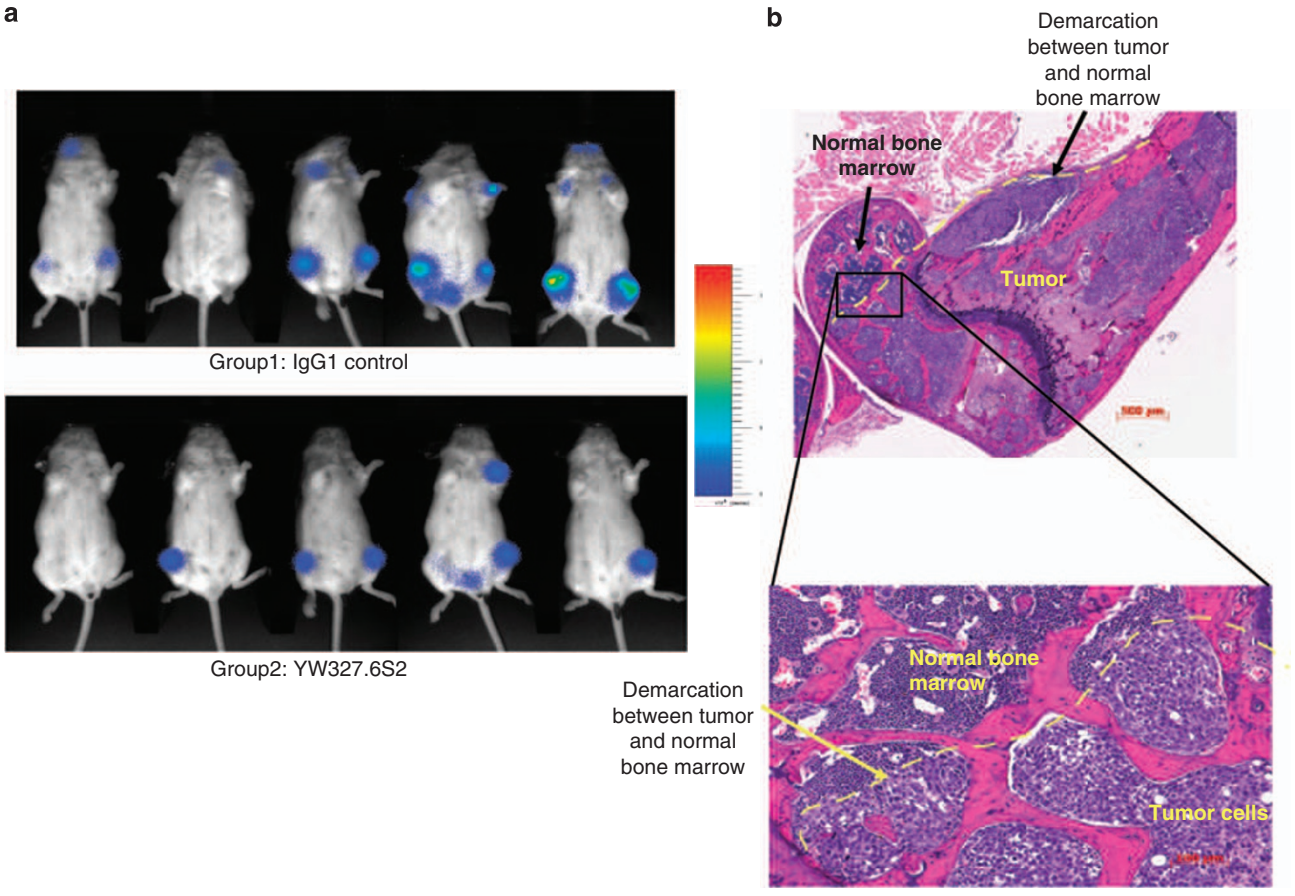

Figure 5 YW327.6S2 reduces the metastasis of MDA-MB-231 breast cancer cells to the bone. (**a**) Bioluminescence imaging 4 weeks after tail vein injection of tumor cells. Mice were injected intraperitoneally with 200 μl of 25 mg/ml D-luciferin (Invitrogen, Carlsbad, CA, USA) in PBS and were anesthetized during imaging using isoflurane through nose cone. Bioluminescence images were acquired using a Photon Imager (Biospace Lab, Paris, France), which has an intensified charge-coupled device camera. (**b**) Hematoxylin and eosin staining of the tibia sections. Tissues were collected at the end of the experiments and fixed in 4% formaldehyde, sectioned and stained with hematoxylin and eosin. The circle in the upper panel shows tumor cells invading the bone. The lower panel shows details of neoplastic cells in the bone marrow. PBS, phosphate-buffered saline.

Discussion

We have developed and characterized a human anti-Axl mAb (YW327.6S2) that exhibits cross-species reactivity and blocks various functions of Axl in tumorigenesis. Besides being the first reported fully humanized blocking antibody for Axl, YW327.6S2 not only serves as a powerful tool to dissect out the effect of Axl activation/signaling in multiple aspects of cancer development and progression, but also represents a potential therapeutic for treatment of various cancers.

Our results show that YW327.6S2 blocks the functions of Axl by downregulation of the expression of Axl as well as through inhibition of ligand Gas6 binding to the receptor, leading to inactivation of Axl and its downstream signaling (Figure 1). The ability of YW327.6S2 to downregulate the expression of Axl in cancer cells represents an important mechanism for its inhibitory effects, as many cancers express constitutively activated Axl and are no longer responsive to exogenous Gas6 (Li *et al*., 2009).

In the A549 NSCLC model, YW327.6S2 significantly attenuated tumor growth when administered as a single agent (Figure 2a). This inhibitory effect is comparable to that of anti-Axl hybridoma antibodies in this model (Li *et al*., 2009, Figure 2c). YW327.6S2 rapidly downregulates the expression of Axl in xenografts (Figure 2d), and induces the apoptosis of tumor cells (Figure 2e), which is likely one of the mechanisms that mediates its inhibitory effect on tumor growth. Our previous findings that Axl modulates endothelial cell functions by regulating the DKK3 and angiopoietin/Tie-2 pathways (Li *et al*., 2009) raised the possibility that an anti-Axl mAb could enhance the effect of anti-VEGF in reducing tumor growth. Our results (Figures 2a and f) are consistent with this hypothesis, in that YW327.6S2 affects tumor vasculature by enhancing the effect of anti-VEGF to reduce intra-tumoral vascular density. Indeed, co-administration of YW327.6S2 and anti-VEGF in the A549 model resulted in tumor stasis that was maintained for at least 4 weeks after treatment cessation (Figure 2b). The hybridoma antibody 12A11 also enhances the antitumor effect of anti-VEGF in this model (Figure 2c). However, unlike YW327.6S2, 12A11 does not have a direct effect on tumor vasculature; rather it directly inhibits tumor cell proliferation and induces apoptosis (20). The effect of 12A11 on tumor growth and the anti-VEGF on tumor vasculature resulted in an increased effect when the two agents are used together.

EGFR small-molecule inhibitors such as erlotinib are efficacious in the treatment of NSCLC tumors that harbor EGFR mutations or amplification (Lynch *et al*., 2004; Paez *et al*., 2004; Giaccone, 2005; Eberhard *et al*., 2005; Tsao *et al*., 2005). It is also known that treatment of breast cancer cells with Her-2/EGFR small-molecule inhibitor lapatinib or the anti-Her2 antibody herceptin induces the expression of Axl and consequently results in resistance of cancer cells to these therapies (Liu *et al*., 2009). We have found recently that expression of Axl is induced in HCC827 NSCLC (a cell line that harbors both EGFR mutation and amplification) cells that have acquired resistance to erlotinib and knockdown of Axl in resistant cells restores their sensitivity to erlotinib (unpublished data), suggesting that Axl may have a role in erlotinib resistance in NSCLC. As A549 cells contains wild-type EGFR and are only moderately sensitive to EGFR inhibition *in vitro* (Yauch *et al*., 2005), we asked whether anti-Axl mAb would sensitize these cells to erlotinib. Our results showed that YW327.6S2 potentiates the effect of erlotinib in reducing tumor growth (Figure 3a), suggesting that anti-Axl mAb may enhance the efficacy of EGFR inhibitors in tumors that are refractory to EGFR inhibition alone, perhaps by directly reducing the expression of Axl in tumor cells.

Systemic chemotherapy plays the largest part in the treatment paradigms for NSCLC. For recurrent or advanced disease, patients treated with chemotherapy, which consists of carboplatin/paclitaxel, have a response rate of 15% and a median survival period of 10.3 months (Sandley *et al*., 2006). Our results using the A549 NSCLC model showed that YW327.6S2 is able to enhance the antitumor efficacy of carboplatin/paclitaxel (Figure 3b), suggesting that blocking the functions of Axl might improve the therapeutic index of chemotherapy in this disease. Our results are consistent with a recent report showing an Axl small-molecule inhibitor synergized with cisplatin to suppress liver micrometa stasis in 4T1 breast cancer orthotopic model (Holland *et al*., 2010).

In the MDA-MB-231 breast cancer model, YW327.6S2 alone is able to significantly attenuate tumor growth (Figure 4a). The anti-Axl hybridoma antibody, which does not cross-react with murine Axl and therefore would only affect tumor cells, has no significant effect on tumor growth in this model (Figure 4b). These results suggest that YW327.6S2 is likely to exert its antitumor effect through its actions on the tumor stroma. Our results show that YW327.6S2 reduces intratumoral vascular density (Figure 4e) and enhances the effect of anti-VEGF. Through its effect on tumor vasculature, YW327.6S2 may affect on tumor growth.

An association between development of cancer and inflammation has long been appreciated (Balkwill and Mantovani, 2001; Coussens and Werb, 2002). The chronic inflammation associated with infection and irritation may lead to environments that foster genomic lesions and tumor initiation. There is increasing evidence that TAMs have causal roles in tumor progression, including promotion of angiogenesis and matrix remodeling (Pollard, 2004; Balkwill *et al*., 2005). The signals responsible for this are thought to be inflammatory cytokines, including tumor necrosis factor-α, interleukin 6 and a plethora of chemokines. These cytokines and chemokines not only recruit immune cells to the specific sites that stimulate tumor progression, but it has been shown that their receptors are expressed on tumor cells where they can increase tumor growth and migration (Haghnegahdar *et al*., 2000). In primary human breast cancer, the Axl protein is expressed at high levels on TAMs (Figure 4f). We provide here

evidence that anti-Axl mAbs could modulate the functions of these cells through an indirect mechanism. Our data showed that treatment of MDA-MB-231 xenografts with either YW327.6S2 or 12A11 (which does not cross-react with murine Axl and therefore should not have direct effect on the TAMs) inhibits the secretion of inflammatory cytokines and chemokines from TAMs (Figure 4g). As Axl mAbs do not seem to have a significant effect on the expression of Axl on TAMs, but downregulate receptor expression on tumor cells, it is likely that anti-Axl mAbs modulate cytokine/chemokine secretion from TAMs by blocking the crosstalk between tumor and stromal cells. These results are consistent with the recent reports that tumor cells could promote their growth by educating infiltrating leukocytes to induce the expression of Gas6 (Loges *et al*., 2010); and a small-molecule inhibitor of Axl reduced the expression of granulocyte macrophage colony-stimulating factor in 4T1 breast tumor cells (Holland *et al*., 2010).

Previous studies have established the role of Axl in promoting tumor cell migration, invasion and metastasis (Vajkoczy *et al*., 2006; Tai *et al*., 2008; Zhang *et al*., 2008; Li *et al*., 2009; Gjerdrum *et al*., 2010). Here we showed that YW327.6S2 is able to reduce the metastasis of MDA-MB-231 breast cancer cells to the bone. These results are consistent with our previous data that silencing of Axl by RNAi in breast cancer cells inhibits their metastasis to the lung in an orthotropic model (Li *et al*., 2009; Gjerdrum *et al*., 2010), suggesting that this anti-Axl antibody could have therapeutic potential not only in the treatment of primary tumor but also in metastatic disease.

In conclusion, we have developed a human mAb that blocks the functions of Axl. This anti-Axl mAb exerts its antitumor effect through multiple mechanisms, including induction of tumor cell apoptosis, regulation of angiogenesis and modulation of tumor-associated immune cells functions. In addition, this anti-Axl mAb enhances the antitumor efficacy of anti-VEGF, EGFR SMI as well as chemotherapy, and may therefore represent a novel therapeutic approach in clinical settings where these therapies are standard care.

Materials and methods

Antibodies and cell lines

Antibodies were obtained from the following suppliers: mouse mAb against human Axl (Abnova, Taipei, Taiwan), phospho-Akt mouse mAb and Akt polyclonal antibody (Cell Signaling, Danvers, MA, USA). Mouse recombinant Gas6 and ELISA kit for phospho-Axl were purchased from R&D Systems (Minneapolis, MN, USA). Human carcinoma cell lines were obtained from ATCC (Manassas, VA, USA) and cultured in RPMI-1640 medium supplemented with 10% fetal bovine serum.

Generation of phage anti-Axl mAbs

For antibody generation, human phage antibody libraries with synthetic diversities in the selected complementary-determining regions (H1, H2 and H3), mimicking the natural diversity of the human IgG repertoire, were used for panning. Fab fragments were displayed bivalently on the surface of M13 bacteriophage particles (Lee *et al*., 2004). The phage antibody libraries were panned against human and murine Axl ECD in alternative rounds. Phage antibodies that bound to human Axl ECD-His and murine Axl ECD-Fc fusion protein were identified by ELISA and DNA sequencing, and antibody clones were reformatted to express full-length IgGs (Liang *et al*., 2007). Individual clones were transiently expressed in mammalian cells and purified using protein-A columns (Carter *et al*., 1992).

Phage clones were screened for their ability to inhibit Gas6-dependent proliferation of Baf3-Axl cells. Two clones that exhibited highest potency in the inhibition of Baf3Axl cell proliferation were chosen for affinity maturation.

For affinity maturation, phagemid displaying monovalent Fab on the surface of an M13 bacteriophage (Liang *et al*., 2007) served as the library template for grafting light chain (V_L) and heavy chain (V_H) variable domains of the phage Ab. A soft randomization strategy was adopted for affinity maturation as described by Liang *et al*. (2007), and a high-throughput, single-point competitive phage ELISA was used to rapidly screen for high-affinity clones as described (Sidhu *et al*., 2004).

Affinity measurement of anti-Axl antibodies

For binding affinity determinations of anti-Axl antibodies, surface Plasmon Resonance measurement with a BIAcore-3000 instrument was used. To measure the affinity between anti-Axl antibodies and the human Axl ECD-His protein, anti-Axl human IgG was captured by CM5 biosensor chips coated with mouse anti-human IgG to achieve approximately 250 response units. For measurements of kinetics, twofold serial dilutions of human Axl ECD-His (440–28 nM) were injected in PBT buffer (phosphate-buffered saline (PBS) with 0.05% Tween 20) at 25 °C with a flow rate of 30 μl/min. Association rates (k_{on}) and dissociation rates (k_{off}) were calculated using a simple one-to-one Langmuir binding model (BIAcore Evaluation Software version 3.2). The equilibrium dissociation constant (K_D) was calculated as the k_{off}/k_{on} ratio. To measure the affinity of anti-Axl antibodies to the murine Axl ECD-Fc fusion protein, the murine Axl ECD human IgG fusion protein was captured by CM5 biosensor chips coated mouse anti-human IgG to achieve approximately 150 response units. For measurements of kinetics, twofold serial dilutions of the anti-Axl Fab fragment (200–12 nM) were injected in PBST buffer (PBS with 0.05% Tween 20) at 25 °C with a flow rate of 30 μl/min.

Cell proliferation assay

Cells were seeded at 5000 cells/well in 96-well plates and treated with an Axl mAb at various concentrations for 72 h. Cell proliferation was measured using a CellTiter-Glo Luminescent Cell Viability Assay (Promega, Madison, WI, USA) according to the manufacturer's instructions.

ELISA and FACS

ELISA and FACS analysis were performed as described previously (Li *et al*., 2009).

Xenograft experiments

All studies were conducted in accordance with the 'Guide for the Care and Use of Laboratory Animals' (NIH) and

approved by the Institutional Animal Care and Used Committee (IACUC).

A total of 5×10^6 (A549) or 10^7 cells in matrigel (MDA-MB-231) were implanted subcutaneously into the right flank of nude (A549) or SCID mice (MDA-MB-231), respectively. When the average tumor sized reached 100 mm^3 mice were randomized and divided into different treatment groups ($n = 10$ for each group). Anti-Axl or control IgG1 antibodies were at administered at 10–30 mg/kg, anti-VEGF at 1–2 mg/kg, by intraperitoneal injection, twice weekly. Erlotinib was administered by oral gavage at 100 mg/kg/day. Paclitaxel and carboplatin were administered subcutaneously at 6.25 mg/kg/day for 5 days and 100 mg/kg for a single dose, respectively, at the beginning of the treatment. Statistic analyses were performed using two-way analysis of variance for comparison of tumor growth in different treatment groups.

For pharmacodynamic studies, mice were treated with antibodies for 0, 24, 72 and 168 h. At each time point, tumors were excised, processed for immunohistochemical staining and image analysis, and used to generate cell lysates for western blot analysis.

For metastasis studies, 5×10^5 MDA-MB-231 cells stably transfected with a luciferase reporter gene (Li *et al*., 2009) were implanted into SCID mice by tail vein injection. Metastasis of tumor cells to various organs was monitored by bioluminescence detection as described by Li *et al*. (2009).

Immunohistochemistry

Xenograft tumor samples were fixed in 10% neutral buffered formalin, processed, embedded in paraffin and sectioned at 4 μm. Thin sections were then treated with primary antibodies for Ki67, cleaved caspase-3 and MECA32, followed by biotinylated secondary antibodies and the DAB chromogen.

Primary human breast cancer tissue microarray was obtained from Cureline Inc. (South San Francisco, CA, USA), including ductal and metastatic adenocarcinomas. Axl IHC was performed using an anti-Axl mAb as described previously (Li *et al*., 2009), and macrophages were stained using CD68. For dual Axl/CD68 IHC, Axl staining was performed first at 2 μg/ml using Vector ABC Elite HRP reagents and a DAB substrate. CD68 staining was run sequentially at 0.5 μg/ml, also using ABC Elite HRP reagents but using a Vector SG chromogen (blue/gray) instead. A second target antigen retrieval step was performed in between the two complexes to elute off the first complex to avoid cross-reactivity of the two markers.

Vascular density measurement and data analysis

Tumor samples were stained with MECA32, a pan endothelial cell marker. Images were acquired using an Ariol SL-50 automated slide scanning platform (Genetix Ltd, Hampshire, UK) at a final magnification of $\times 100$. Tumor-specific areas were exported for analysis in the Metamorph software package (MDS Analytical Technologies, ON, Canada) as individual 8-bit images. The brown DAB-specific staining was isolated from the hematoxylin counterstain using a blue-normalization algorithm as described by Brey *et al*. (2003). A segmentation algorithm identified vessels and removed noise on the basis of size and shape. Cells were identified as either tumor or non-tumor on the basis of size, shape and density of hematoxylin staining. Non-tumor areas were identified by the density of non-tumor cells versus tumor cells. After analysis was complete, images were reviewed manually to remove artifacts identified incorrectly as vessels or tumor areas. Area measurements were recorded for individual vessels, as well as the tumor and non-tumor areas in each image. Raw values on the basis of image analysis were analyzed using the JMP 8.0 software (SAS Institute Inc., Cary, NC, USA). A Student's *t*-test was performed to compare each pair of means, with $P < 0.05$.

Isolation of TAMs and detection of secreted cytokines

Tumors were dissected, chopped into small pieces and incubated in RPMI-1640 medium with 2.5% fetal bovine serum, 0.2 U/ml Liberase Blendzymes-II and 5 U/ml DNase-I (Roche, Pleasonton, CA, USA). Tumor cells were disassociated using an MACS Dissociator (Miltenyi Biotec, Bergisch Gladbach, Germany) and maintained for 20 min at room temperature. EDTA (final concentration 0.002%) was added to stop the reaction. Single-cell suspensions were prepared and red blood cells were removed using an RBC lysis buffer (eBioscience, San Diego, CA, USA). Cells were resuspended at 10^7 cells/ml in PBS containing 1% fetal bovine serum and incubated with 20 μg/ml FcRII, III and IV for 20 min. Anti-F4/80-PE (eBioscience) and anti-CD11c-APC (BD Pharmingen, San Jose, CA, USA) (0.2 μg/10^6 cells) were added and incubated for 30 min on ice. F4/80 and CD11c-positive cells were sorted by FACSAria (BD Biosciences, San Jose, CA, USA). A total of 2×10^5 F4/80 and CD11c-positive cells were seeded in a 96-well plate and cultured overnight. The culture media was collected and the levels of cytokines and chemokines were determined using Bio-Plex mouse cytokine assays (Bio-Rad, Hercules, CA, USA) according to the manufacturer's instructions.

Conflict of interest

The authors declare no conflict of interest. The authors are all employees of Genentech.

Acknowledgements

We thank Dr Jiping Zha for developing the dual anti-Axl/CD68 IHC protocol.

References

Balkwill F, Charles KA, Mantovani A. (2005). Smoldering and polarized inflammation in the initiation and promotion of malignant disease. *Cancer Cell* **7**: 211–217.

Balkwill F, Mantovani A. (2001). Inflammation and cancer: back to Virchow? *Lancet* **357**: 539–545.

Berclaz G, Altermatt HJ, Rohrbach V, Kieffer I, Dreher E, Andres AC. (2001). Estrogen dependent expression of the receptor tyrosine kinase axl in normal and malignant human breast. *Ann Oncol* **12**: 819–824.

Brey EM, Lalani Z, Johnston C, Wong M, McIntire LV, Duke PJ *et al*. (2003). Automated selection of DAB-labeled tissue for immunohistochemical quantification. *J Histochem Cytochem* **51**: 575–584.

Carter P, Presta L, Gorman CM, Ridgway JB, Henner D, Wong WL *et al*. (1992). Humanization of an anti-p185HER2 antibody for human cancer therapy. *Proc Natl Acad Sci USA* **89**: 4285–4289.

Chung BI, Malkowicz SB, Nguyen TB, Libertino JA, McGarvey TW. (2003). Expression of the proto-oncogene Axl in renal cell carcinoma. *DNA Cell Biol* **22**: 533–540.

Coussens LM, Werb Z. (2002). Inflammation and cancer. *Nature* **420**: 860–867.

Craven RJ, Xu LH, Weiner TM, Fridell YW, Dent GA, Srivastava S *et al*. (1995). Receptor tyrosine kinases expressed in metastatic colon cancer. *Int J Cancer* **60**: 791–797.

Eberhard DA, Johnson BE, Amler LC, Goddard AD, Heldens SL, Herbst RS *et al*. (2005). Mutations in the epidermal growth factor receptor and in KRAS are predictive and prognostic indicators in patients with non-small cell lung cancer treated with chemotherapy alone and in combination with erlotinib. *J Clin Oncol* **23**: 5900–5909.

Giaccone G. (2005). Epidermal growth factor receptor inhibitors in the treatment of non-small-cell lung cancer. *J Clin Oncol* **23**: 3235–3242.

Gjerdrum C, Tiron C, Hoiby T, Stefansson I, Haugen H, Sandal T *et al*. (2010). Axl is an essential epithelial-to-mesenchymal transition-induced regulator of breast cancer metastasis and patient survival. *Proc Natl Acad Sci USA* **107**: 1124–1129.

Haghnegahdar H, Du J, Wang D, Strieter RM, Burdick MD, Nanney LB *et al*. (2000). The tumorigenic and angiogenic effects of MGSA/GRO proteins in melanoma. *J Leukoc Biol* **67**: 53–62.

Holland SJ, Pan A, Franci C, Hu Y, Chang B, Li W *et al*. (2010). R428, a selective small molecule inhibitor of Axl kinase, blocks tumor spread and prolongs survival in models of metastatic breast cancer. *Cancer Res* **70**: 1544–1554.

Holland SJ, Powell MJ, Franci C, Chan EW, Friera AM, Atchison RE *et al*. (2005). Multiple roles for the receptor tyrosine kinase axl in tumor formation. *Cancer Res* **65**: 9294–9303.

Hong CC, Lay JD, Huang JS, Cheng AL, Tang JL, Lin MT *et al*. (2008). Receptor tyrosine kinase AXL is induced by chemotherapy drugs and overexpression of AXL confers drug resistance in acute myeloid leukemia. *Cancer Lett* **268**: 314–324.

Hutterer M, Knyazev P, Abate A, Reschke M, Maier H, Stefanova N *et al*. (2008). Axl and growth arrest-specific gene 6 are frequently overexpressed in human gliomas and predict poor prognosis in patients with glioblastoma multiforme. *Clin Cancer Res* **14**: 130–138.

Ito T, Ito M, Naito S, Ohtsuru A, Nagayama Y, Kanematsu T *et al*. (1999). Expression of the Axl receptor tyrosine kinase in human thyroid carcinoma. *Thyroid* **9**: 563–567.

Janssen JW, Schulz AS, Steenvoorden AC, Schmidberger M, Strehl S, Ambros PF *et al*. (1991). A novel putative tyrosine kinase receptor with oncogenic potential. *Oncogene* **6**: 2113–2120.

Koorstra JB, Karikari CA, Feldmann G, Bisht S, Rojas PL, Offerhaus GJ *et al*. (2009). The Axl receptor tyrosine kinase confers an adverse prognostic influence in pancreatic cancer and represents a new therapeutic target. *Cancer Biol Ther* **8**: 618–626.

Lai C, Lemke G. (1991). An extended family of protein-tyrosine linase genes differentially expressed in the vertebrate nervous system. *Neuron* **6**: 691–704.

Lee CV, Liang WC, Dennis MS, Eigenbrot C, Sidhu SS, Fuh G. (2004). High-affinity human antibodies from phage-displayed synthetic Fab libraries with a single framework scaffold. *J Mol Biol* **340**: 1073–1093.

Li Y, Ye X, Tan C, Hongo JA, Zha J, Liu J *et al*. (2009). Axl as a potential therapeutic target in cancer: role of Axl in tumor growth, metastasis and angiogenesis. *Oncogene* **28**: 3442–3455.

Liang WC, Wu X, Peale FV, Lee CV, Meng YG, Gutierrez J *et al*. (2006). Cross-species vascular endothelial growth factor (VEGF)-blocking antibodies completely inhibit the growth of human tumor xenografts and measure the contribution of stromal VEGF. *J Biol Chem* **281**: 951–961.

Liang WC, Dennis MS, Stawicki S, Chanthery Y, Pan Q, Chen Y *et al*. (2007). Function blocking antibodies to neuropilin-1 generated from a designed human synthetic antibody phage library. *J Mol Biol* **366**: 815–829.

Liu L, Greger J, Shi H, Liu Y, Greshock J, Annan R *et al*. (2009). Novel mechanism of lapatinib resistance in HER2-positive breast tumor cells: activation of AXL. *Cancer Res* **69**: 6871–6878.

Loges S, Schmidt T, Tjwa M, van Geyte K, Lievens D, Lutgens E *et al*. (2010). Malignant cells fuel tumor growth by educating infiltrating leukocytes to produce the mitogen Gas6. *Blood* **115**: 2264–2273.

Lynch TJ, Bell TW, Sordella R, Gurubhagavatula S, Okimoto RA, Brannigan BW *et al*. (2004). Activating mutations in the epidermal growth factor receptor underlying responsiveness of non-small-cell lung cancer to gefitinib. *N Engl J Med* **350**: 2129–2139.

Mahadevan D, Cooke L, Riley C, Swart R, Simons B, Della Croce K *et al*. (2007). A novel tyrosine kinase switch is a mechanism of imatinib resistance in gastrointestinal stromal tumors. *Oncogene* **26**: 3909–3919.

Meric F, Lee WP, Sahin A, Zhang H, Kung HJ, Hung MC. (2002). Expression profile of tyrosine kinases in breast cancer. *Clin Cancer Res* **8**: 361–367.

O'Bryan JP, Frye RA, Cogswell PC, Neubauer A, Kitch B, Prokop C *et al*. (1991). Axl, a transforming gene isolated from primary human myeloid leukemia cells, encodes a novel receptor tyrosine kinase. *Mol Cell Biol* **11**: 5016–5031.

Paez JG, Janne PA, Lee JC, Tracy S, Greulich H, Gabriel S *et al*. (2004). EGFR mutations in lung cancer: correlation with clinical response to gefitinib therapy. *Science* **304**: 1497–1500.

Pollard JW. (2004). Tumour-educated macrophages promote tumour progression and metastasis. *Nat Rev Cancer* **4**: 71–78.

Rikova K, Guo A, Zeng Q, Possemato A, Yu J, Haack H *et al*. (2007). Global survey of phosphotyrosine signaling identifies oncogenic kinases in lung cancer. *Cell* **131**: 1190–1203.

Sainaghi PP, Castello L, Bergamasco L, Galletti M, Bellosta P, Avanzi GC. (2005). Gas6 induces proliferation in prostate carcinoma cell lines expressing the Axl receptor. *J Cell Physiol* **204**: 36–44.

Sandler A, Gray R, Perry MC, Brahmer J, Schiller JH, Dowlati A *et al*. (2006). Palitaxel–carboplatin alone or with bevacizumab for non-small cell lung cancer. *N Engl J Med* **355**: 2542–2550.

Shieh YS, Lai CY, Kao YR, Shiah SG, Chu YW, Lee HS *et al*. (2005). Expression of axl in lung adenocarcinoma and correlation with tumor progression. *Neoplasia* **7**: 1058–1064.

Sidhu SS, Li B, Chen Y, Fellouse FA, Eigenbrot C, Fuh G. (2004). Phage-displayed antibody libraries of synthetic heavy chain complementarity determining regions. *J Mol Biol* **338**: 299–310.

Sun W, Fujimoto J, Tamaya T. (2004). Coexpression of Gas6/Axl in human ovarian cancers. *Oncology* **66**: 450–457.

Tai KY, Shieh YS, Lee CS, Shiah SG, Wu CW. (2008). Axl promotes cell invasion by inducing MMP-9 activity through activation of NF-kappaB and Brg-1. *Oncogene* **27**: 4044–4055.

Tsao MS, Sakurada A, Cutz JC, Zhu CQ, Kamel-Reid S, Squire J *et al*. (2005). Erlotinib in lung cancer—molecular and clinical predictors of outcome. *N Engl J Med* **353**: 133–144.

Vajkoczy P, Knyazev P, Kunkel A, Capelle HH, Behrndt S, von Tengg-Kobligk H *et al*. (2006). Dominant-negative inhibition of the Axl receptor tyrosine kinase suppresses brain tumor cell growth and invasion and prolongs survival. *Proc Natl Acad Sci USA* **103**: 5799–5804.

Wu CW, Li AF, Chi CW, Lai CH, Huang CL, Lo SS *et al*. (2002). Clinical significance of AXL kinase family in gastric cancer. *Anticancer Res* **22**: 1071–1078.

Yauch RL, Januario T, Eberhard DA, Cavet G, Zhu W, Fu L *et al*. (2005). Epithelial versus mesenchymal phenotype determines in vitro sensitivity and predicts clinical activity of erlotinib in lung cancer patients. *Clin Cancer Res* **11**: 8686–8698.

Zhang YX, Knyazev PG, Cheburkin YV, Sharma K, Knyazev YP, Orfi L *et al*. (2008). AXL is a potential target for therapeutic intervention in breast cancer progression. *Cancer Res* **68**: 1905–1915.